HYDROLOGICAL PROCESSES, VOL. 11, 1945–1961 (1997)

EVALUATION OF THE POST-MINING GROUNDWATER REGIME FOLLOWING LONGWALL MINING

J. LIU,[1]* D. ELSWORTH[2] AND R. J. MATETIC[3]

[1]*Department of Mining, Minerals and Materials Engineering, University of Queensland, Brisbane, QLD 4072, Australia*
[2]*Department of Mineral Engineering, Pennsylvania State University, University Park, PA 16802, USA*
[3]*US Department of Energy, Pittsburgh Research Center, Pittsburgh, PA 15236, USA*

ABSTRACT

A methodology for calculating strains that accompany mining is used to estimate the post-mining modification of the hydraulic conductivity field and the change in the regional and local subsurface water system. The techniques yield reasonable agreement with recorded changes in water levels for reasonable and defensible choices of material parameters in validation exercises at an instrumented longwall site. Water level changes recorded above the twin panel longwall configuration are complex and varied. However, they may be explained through consideration of the mining-modified conductivity field alone. Changes in hydraulic conductivity are independently corroborated from the results of *in situ* permeability tests, conducted before and after mining, that confirm the overall influence of mining-induced strains. These resulting patterns of hydraulic conductivity enhancement enable direct explanation of observed water level changes.

Hydrol. Process., Vol. 11, 1945–1961 (1997)

(No. of Figures: 16 No. of Tables: 2 No. of Refs: 12)

KEY WORDS mining hydrology; coupled flow deformation; subsidence; finite element; fracture hydrology; longwall mining

INTRODUCTION

Underground mining by full extraction methods, such as longwall mining, is becoming increasingly popular for mining uninterrupted and near-horizontal seams. Longwall mining involves extracting coal in large blocks, called panels, using a mechanized shearer. The full thickness, of perhaps 1–2 m, is removed and panel extents are typically 200–350 m wide and up to 3000 m in length. Multiple panels comprise a single mining operation. With this method, the mine roof is supported with hydraulic supports that automatically advance as mining progresses. As the supports move, the mine roof is allowed to collapse into the mine void. Strata above the mine level are altered as the mine roof caves behind the shields (hydraulic supports), creating zones where blocks of rock fill the mine void, or fracture or deform as rock layers warp downwards. These alterations in overburden characteristics potentially induce large strains in the overlying strata that in turn may result in a strongly heterogeneous and anisotropic hydraulic conductivity field. This strain-dependent conductivity field is of special importance in evaluating the potential impact of longwall mining on groundwater resources. A number of studies have indicated that subsidence-induced fracturing may increase hydraulic conductivity magnitudes by up to several orders of magnitude (Neate and Whittaker, 1979; Booth, 1992). Consequently, the local groundwater system may be appreciably altered (Matetic and Trevits, 1990, 1992; Matetic, 1993). Despite the acknowledgement that changes in conductivity may be substantial, few studies document the interaction between deformation of the overlying strata and its influence on groundwater flow (Ouyang and Elsworth, 1993; Liu, 1994). The following documents an

* Correspondence to: J. Liu.

Contract grant sponsors: National Science Foundation and National Mined Land Reclamation Center.
Contract grant numbers: CMS-9209059 and CO388962.

CCC 0885–6087/97/151945–17$17·50

Received 22 January 1996
Accepted 24 October 1996

approach to define the form of this interaction, in a predictive capacity, enabling the influence on the groundwater system to be defined.

The undermined strata typically have a complicated internal structure and stress state, both of which are, in large part, unknown and perhaps unknowable. This would appear to make solution of the revised, mining-induced, conductivity field intractable. However, some alternatives may be pursued to avoid using parameters that are unlikely to be available in practice. The subsidence field that develops around a longwall panel is insensitive to deformation modulus or strength (Elsworth *et al.*, 1994; Liu, 1994). Therefore, the mining-induced strain field, defined by the subsidence profile, may also be decoupled from the material parameters describing the overlying strata. Once the strain field is defined uniquely for a given mining geometry, changes in the groundwater system may be evaluated, if a link can be established between induced strains and changes in hydraulic conductivity. This is the underlying scientific rationale for this work.

METHODOLOGY

The potential impact of longwall mining on groundwater resources is evaluated through the following straightforward steps.

- The strain field that develops around a longwall panel as a result of mining is defined using a finite element model that accommodates the influence of material failure and gravitational body force.
- From this calculated strain field, and from knowledge of the pre-mining hydraulic properties of the overlying strata, the change in hydraulic conductivity that results from the strain field may be determined.
- With the modified conductivity field determined, the post-mining hydrological system may subsequently be defined through application of a groundwater model. Again, this groundwater model utilizes the finite element method to determine the post-mining hydrological system, where the change in the position of the piezometric surface indicates changes in well or aquifer yields.

Finite element formulation

The resulting finite element formulation may be symbolically defined as

$$\begin{pmatrix} \boldsymbol{K}_s & 0 \\ 0 & \boldsymbol{K}_f \end{pmatrix} \begin{Bmatrix} \boldsymbol{d} \\ \boldsymbol{h} \end{Bmatrix} = \begin{Bmatrix} \boldsymbol{f} \\ \boldsymbol{q} \end{Bmatrix} \tag{1}$$

where $\boldsymbol{K}_s$ is the stiffness matrix to define solid body deformations, $\boldsymbol{K}_f$ is the conductance matrix of the fluid phase, $\boldsymbol{d}$ is the nodal displacement vector, $\boldsymbol{h}$ is the nodal head vector, $\boldsymbol{f}$ is the nodal force vector and $\boldsymbol{q}$ is the nodal flux vector. This representation enables the important contribution of changes in the strain field $(\varepsilon_x, \varepsilon_y)$ to be determined and applied to the conductivity field $K = f(\varepsilon_x, \varepsilon_y)$.

Coupling between mining-induced strain and conductivity

Equation (1) is a diagonal matrix system and therefore, by definition, fluid flow is decoupled from solid deformation. Thus, body forces resulting from head gradients are neglected, although the important influence of solid deformation on the magnitude of the hydraulic conductivity tensor is incorporated. The coupling is achieved by assuming the dominant influence of fracture permeability and applying a simple relationship linking hydraulic conductivity and solid strain as (Ouyang and Elsworth, 1993),

$$K_x = K_{x0}\left[1 + \frac{b + s(1 - R_m)}{b}\Delta\varepsilon_y\right]^3 \tag{2}$$

$$K_y = K_{y0}\left[1 + \frac{b + s(1 - R_m)}{b}\Delta\varepsilon_x\right]^3 \tag{3}$$

where K_x and K_y are post-mining conductivities in the x- and y-directions, K_{x0} and K_{y0} are the pre-mining conductivities in the x- and y-directions, b and s are fracture aperture and spacing, respectively, $\Delta\varepsilon_x$ and $\Delta\varepsilon_y$ are the mining-induced strains in the x- and y-directions. This behaviour assumes the matrix blocks are impermeable and that conductivity is defined by an equivalent porous medium comprising fractures that behave as parallel-sided conduits of uniform mean spacing, and appropriate hydraulic aperture. Deformation of the assemblage is conditioned by stiffness of the fractures and modulus of the matrix blocks in a linear assemblage. R_m is a modulus reduction ratio [ratio of the modulus of the bulk mass (including fractures) to the modulus of the intact and unfractured matrix] that apportions the changes in strain between the fracture and matrix material. When $R_m = 1$, the mass and intact material moduli are identical and the strain is uniformly distributed between fractures and matrix. This results in the smallest possible change in conductivity. When $R_m = 0$, the extensional strain is applied entirely to the fracture system and precipitates the largest possible change in conductivity. These values bound the possible ranges in behaviour of the system in a natural, and mechanistically defensible manner. This representation of conductivities is extremely useful, since the modulus reduction factor, R_m, may be readily evaluated from rock mass classification systems (Ouyang and Elsworth, 1993) defining structural behaviour as a function of readily observable factors of rock structure. This avoids the difficulty of defining conductivity enhancement in terms of the component moduli of fractures and matrix, parameters that are unlikely to be available in practice.

Material models

The representation of coal extraction, overburden failure and the development of a free surface for groundwater flow is realized through employing different material models for each of the physical processes. These material models are shown in Figure 1.

A bimodulus model is used to represent the failure of overburden materials, as shown in Figure 1a. The model may be expressed as

$$E = \begin{cases} E_1 & \sigma_1 < 0 \\ E_2 & \sigma_1 \geqslant 0 \end{cases} \tag{4}$$

$$\mu = \begin{cases} \mu_1 & \sigma_1 < 0 \\ \mu_2 & \sigma_1 \geqslant 0 \end{cases} \tag{5}$$

where E is the elastic modulus of the overburden, E_1 is the elastic modulus of the elements in compression, E_2 is the elastic modulus of the elements in extension, μ is the Poisson's ratio of the overburden, μ_1 is the Poisson's ratio of the elements in compression, μ_2 is the Poisson's ratio of the elements in extension and σ_1 is the maximum principle stress. The magnitude of E_2 is typically set to between one-third and one-fifth of E_1 by matching the 'field-measured' maximum subsidence based on past experiences. μ_2 is typically set to 0·45 to represent incompressible behaviour in the post-failure regime.

A similar bimodulus model is used to represent the process of coal extraction, as shown in Figure 1a. This is defined as

$$E_{\text{panel}} = \begin{cases} E_0 & \varepsilon_y > -1{\cdot}0 \\ 10^n E_0 & \varepsilon_y \leqslant -1{\cdot}0 \end{cases} \tag{6}$$

where E_{panel} is the modulus of the hypothetical material comprising the panel, E_0 is the initial modulus of the panel material (before mining) and ε_y is the vertical strain within the panel material. This simple model prevents the interpenetration of the panel roof and floor by changing the panel modulus at contact, where n is typically set to 10.

As the induced strain field typically changes the distribution of hydraulic conductivity magnitudes in all adjacent elements, traditional methods of representing the free surface by remeshing are inappropriate. Alternatively, a biconductivity model (Bathe and Khoshgoftaar, 1979) is used to represent desaturation of

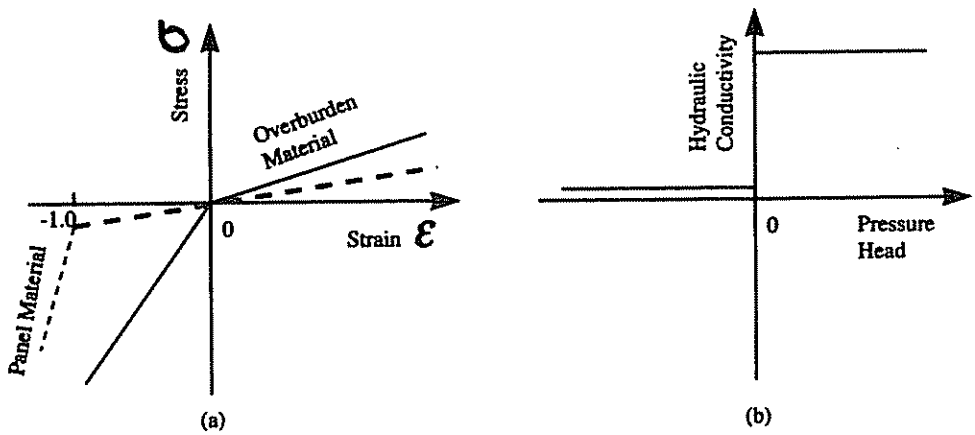

Figure 1. Material models used in the evaluation of mechanical and flow behaviour

the overburden strata and enable representation of the groundwater free surface, as shown in Figure 1b. In the iterative search for a stable free surface configuration, elements containing nodes with heads lower than the elevation head (subatmospheric pressures) are 'switched-off' by assigning a low hydraulic conductivity. This isolates the phreatic surface as a 'no-flow' boundary and has the advantage that remeshing is not required to conform to the iteratively reconfigured saturated flow geometry. This simple, but effective, model may be expressed as

$$K = \begin{cases} K_1 & h > z \\ 10^{-n} K_1 & h \leqslant z \end{cases} \tag{7}$$

where K is the hydraulic conductivity of the overburden, K_1 is the hydraulic conductivity of elements below the groundwater table, h is the total head and z is the elevation head. The magnitude of n is typically set between 3 and 5.

The methodology, outlined above, was successfully applied to the study of an active coal mine as discussed below.

APPLICATION

An intensive surface, subsurface and groundwater monitoring programme was conducted at a research site in south-eastern Ohio. The basic parameters, required by the methodology described previously, *viz.* the subsidence profile and pre-mining conductivity magnitudes, were recorded together with the post-mining hydraulic conductivity field and water level fluctuations throughout mining. The modelling methodology is used to predict the ratios of post- to pre-mining conductivities, and the relative change in water levels recorded in monitoring wells. These comparisons demonstrate the capabilities of the developed procedure to evaluate the potential impact of longwall mining on groundwater resources.

Site specification and field monitoring

Mining plan. The study site is located in south-eastern Ohio (Vinton County). The study area overlies a portion of two contiguous longwall panels (Panel Nos. 1 and 2) measuring approximately 275 m wide and 2743 m long, in plan view. The panels are separated by a five-entry, four-pillar system approximately 107 m wide, as shown in the 'gate entries' of Figure 2. The mined coalbed has an average thickness of 1·4 m within the study area. Overburden thickness is shallow and ranges from 65 to 85 m. Overall, the strata are near-horizontal with a regional dip of about 1 degree towards the south-east. There are no major geological

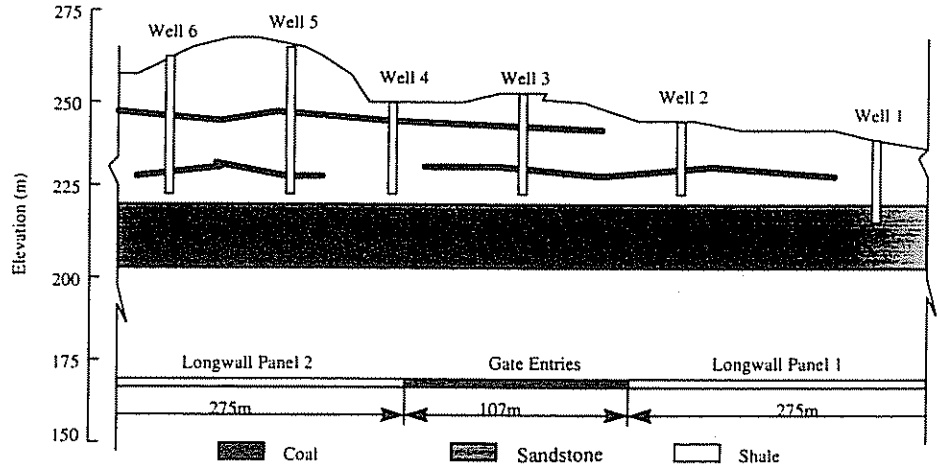

Figure 2. Generalized cross-section of the study area. Panels are mined in the direction, into the page

structures and the surface topography consists mainly of rolling hills with a maximum relief of approximately 50 m.

Geological setting. The geological setting of the study area is typical of that found in south-eastern Ohio. The regional dip in this part of the state is to the south-east, with the strata striking in a north-east–south-west direction. The average rate of dip is 5·6 m per kilometre. Irregularities to this rate can be experienced by localized thinning or thickening of individual rock units. The rock is predominantly interbedded sandstones, shales, thin coal seams and claystones. The individual units are thin (less than 3 m thick) with one sandstone unit having an average thickness of 14 m and lying 43 m above the Clarion 4A Coalbed. To characterize overbuden lithology prior to drilling the water wells, six NX-sized core holes (diameter 5 cm) were drilled to the Clarion 4A Coalbed in the study area. Generally, the overburden consists of about 30% sandstone, 30% shale, 30% clay and 10% coal. A generalized cross-section of the study area with the water well locations is shown in Figure 2.

Field subsidence profile. The field subsidence profile was obtained by monitoring the surface deformation. To obtain the field subsidence profile, survey monuments were installed at the ground surface and were surveyed regularly to identify the dynamic characteristics of subsidence and the final subsidence profile. The array of monuments consisted of two baselines (along the centre-line over each panel) and a profile line running perpendicular between the two baselines. The spacing of the monuments was 15 m apart along each baseline. The profile line was 375 m long, with monuments 7·5 m apart.

Hydrogeology. A comprehensive groundwater monitoring programme was conducted at the mining site using a total of seven 22 cm water wells drilled specifically for the study. These wells were strategically placed above both longwall panels as shown in Figures 2 and 3. Perforated schedule 80 (15 cm diameter) PVC casing was installed to the total depth in each well to ensure an open well-bore for the life of the study. Wells 1–6 were completed within the uppermost shale unit, with only the basal sections penetrating the lower sandstone, as shown in Figure 2. Correspondingly, with all wells open for the full length of penetration and with no seals present, the raw, pre-mining conductivity values, presented in Table I, were assumed indicative of the higher conductivity sandstone layers (Matetic *et al.*, 1995). Calibration studies with the initial pre-mining groundwater surface were used to evaluate the conductivity of the overlying shale layer.

The wells are located along a line perpendicular to the trend of the longwall panels. This alignment permitted observations of effects during the mining of both panels. Well Nos. 1 and 6 are located at the

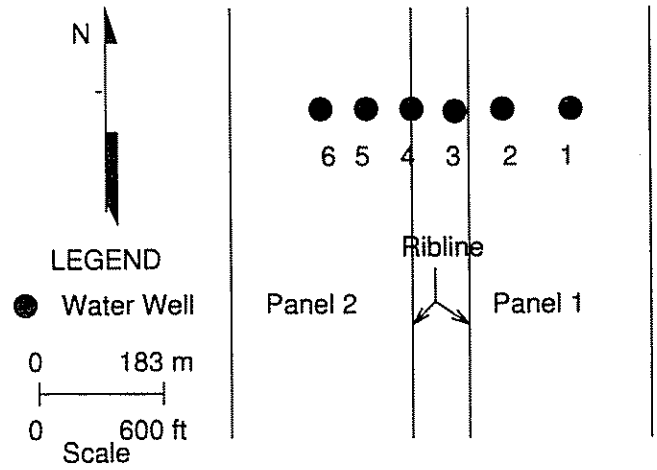

Figure 3. Schematic of study area

centre of panel Nos. 1 and 2, respectively. Well Nos. 2 and 5 are located at quarter-panel width. Well No. 3 is located above the gate roads between the two panels and well No. 4 is located above the edge of panel No. 2. Data were collected from all wells before, during and after mining of both longwall panels. Various hydrological parameters were determined, and included specific capacity, transmissivity, hydraulic conductivity and water level fluctuations. Initial data collection began three months prior to the undermining of well No. 1 to establish reasonable baseline conditions. Drawdown and recovery pumping tests were performed on all wells before and after undermining to determine the hydraulic conductivity parameters of the local, shallow geological units. Electronic recorders were also installed on all wells to monitor water level fluctuations continuously.

Evaluation of the post-mining groundwater regime is based on this intensive surface, subsurface and groundwater monitoring programme. The mining-induced strain field is defined through matching the field subsidence profile. The post-mining conductivity field is determined on the basis of the constrained evaluation of strains through applying one constraint to the system, namely, the flow rate entering the mine following mining of both panels. This is estimated from the known in-mine pumping rates. Consequently, the water level fluctuations are evaluated. These simulated results are compared with the measured results.

Subsidence profile evaluation

The field subsidence profile is determined from the numerical model as shown in Figure 4a. The general cross-section of the study area, as shown in Figure 2, is only a small portion (between two panel centre-lines) of this model. The real topography and mining geometry are incorporated in the model, together with the single 'fitting' parameter, R_m, which is not directly available from the field study. The finite element mesh is

Table I. Drilling depth and measured pre-mining hydraulic conductivities for wells 1–6

Well no.	Drilling depth (m)	Hydraulic conductivity (m/s)
1	17·1	$6{\cdot}7 \times 10^{-5}$
2	16·5	$4{\cdot}1 \times 10^{-5}$
3	22·5	$4{\cdot}0 \times 10^{-5}$
4	27·9	$3{\cdot}1 \times 10^{-5}$
5	38·4	$2{\cdot}5 \times 10^{-5}$
6	36·9	$4{\cdot}1 \times 10^{-5}$

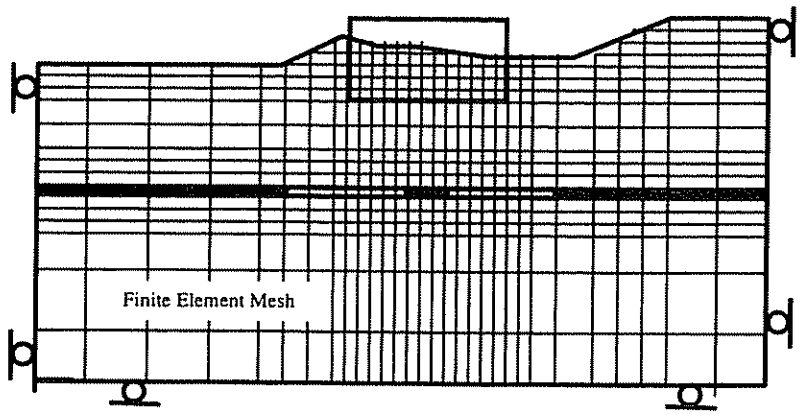

(a) FE model for subsidence evaluation

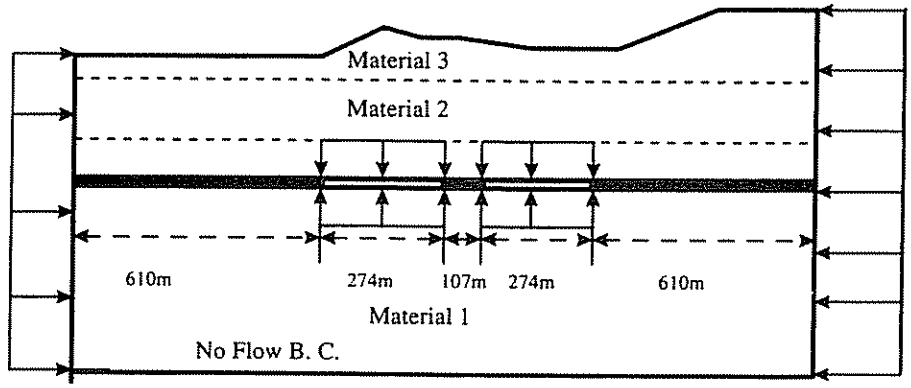

Figure 4. FE models for subsidence and flow simulation. Upper model defines displacement conditions around model periphery. Rollered boundaries represent zero displacement perpendicular to the boundary. Lower model defines hydraulic conditions. Arrows represent prescribed constant head conditions. Inset defines local well-field study defined in Figure 15

constructed of 2066 nodes and 1928 elements. The boundary conditions of the model assume no horizontal movement on either side of the mesh and no vertical movement along the base. A surface free of normal and shear stresses is applied, as a boundary condition, around the panel cavity with loading applied by 'self-weight' of the overburden material owing to gravitational body force. Closure at the panel periphery is allowed until contact between roof and floor occurs, when interpenetration is halted through application of a large interface modulus. The values of the modulus of elasticity for the overburden are based on the laboratory experimental results obtained from core samples collected at the field site. To obtain the model input modulus, an average of all field samples, $3{\cdot}38 \times 10^{10}$ Pa, were calculated and a ratio of 1 : 20 for the overburden material, $1{\cdot}69 \times 10^{9}$ Pa, and 1 : 200 for the coal material, $1{\cdot}69 \times 10^{8}$ Pa, were applied to the experimental results. These ratios reflect the difference between the mechanical properties of the rock mass and the experimental results. They are not important since the developed FE (finite element) model is not sensitive to the material properties of deformation modulus and strength (Liu, 1994). Subsidence deformations are controlled by the ultimate contact between the panel roof and the floor. This displacement control on behaviour renders the problem surprisingly insensitive to the material properties (Elsworth and Liu, 1995). An average Poisson's ratio of 0·30 was used. The post-failure values of the Poisson's ratio and elastic modulus in extensional elements, are 0·45 and $E/4$, respectively, with a no-tension criterion applied to failure.

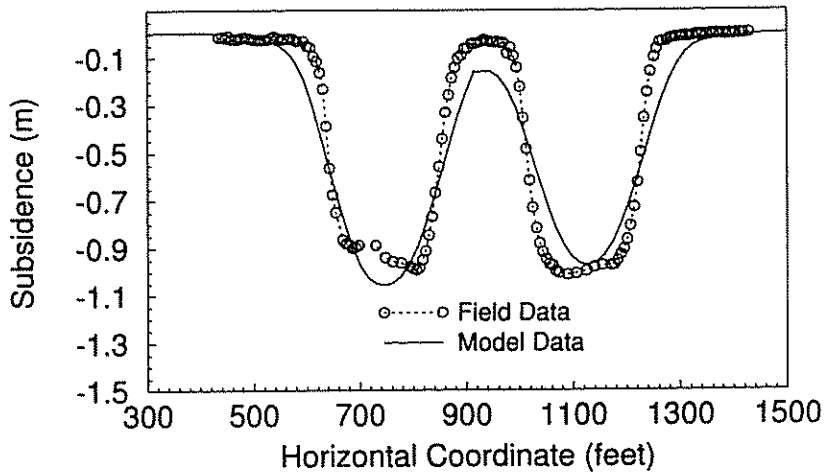

Figure 5. Comparison of model data with field subsidence data

The evaluated subsidence profile is compared with the field subsidence profile in Figure 5. The subsidence profiles above the two panels are different, although their mining geometries are identical. This asymmetry may indicate the presence of heterogeneities within the overburden strata, some subtleties in behaviour not accommodated in the current behavioural model or may result from the direct influence of the overlying topography. Whichever of these causes is operational, the mismatch between the measured and predicted subsidence profiles is not great and this match is considered adequate for the subsequent analyses.

Determination of post-mining groundwater regime

The boundary conditions applied in the evaluation of the post-mining groundwater regime are illustrated in Figure 4b. The true topography, mining geometry and lithology are incorporated in the model. The finite element (FE) mesh is identical to that applied in defining the strain field, merely as an extension of the procedure. The following parameter estimates were used.

Boundary conditions. The boundary conditions for the regional groundwater model were determined from the pre-mining water level elevations recorded in the monitoring wells (Matetic and Trevits, 1990 and 1992). Both the pre-mining and the post-mining groundwater levels recorded in the six wells are shown in Figure 6. The relative change of groundwater level between the six wells is less than 10 m. The pre-mining water level in well No. 1 is the same as that in well No. 6, allowing constant head conditions to be specified on both lateral sides. A no-flow boundary was applied to the bottom of the mesh, and elevation head conditions were applied around the two panels.

Infiltration rates. The infiltration rates for the regional groundwater model were estimated from precipitation records provided by the mining company. The monthly precipitation data (departure from the 50-year average) for the study area are shown in Figure 7 (zero represents the initiation of the study). When the study began, the region was experiencing a drought. The initial portions of the study were conducted when precipitation was less than the 50-year average. In fact, for four months prior to the initiation of the study, the amount of precipitation was less than the 50-year average. In the time following undermining of panel No. 1 when the tests were conducted (days 505 to 515), the area had recovered from the drought. This trend generally continued throughout the remainder of the study. An average precipitation of 1 m/y over the period of the study was used in the FE model. The net infiltration rate, accommodating evapotranspiration, was estimated to be 25% of the total precipitation occurring at the site (0·25 m). The total infiltration quantity was $1{\cdot}50 \times 10^{-5}$ $m^3/s \cdot m^2$.

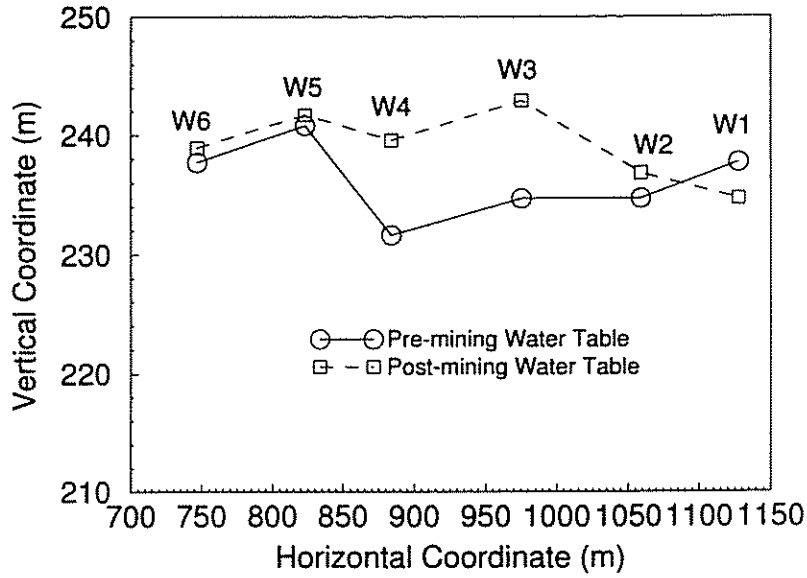

Figure 6. Pre-mining and post-mining groundwater levels in monitoring wells

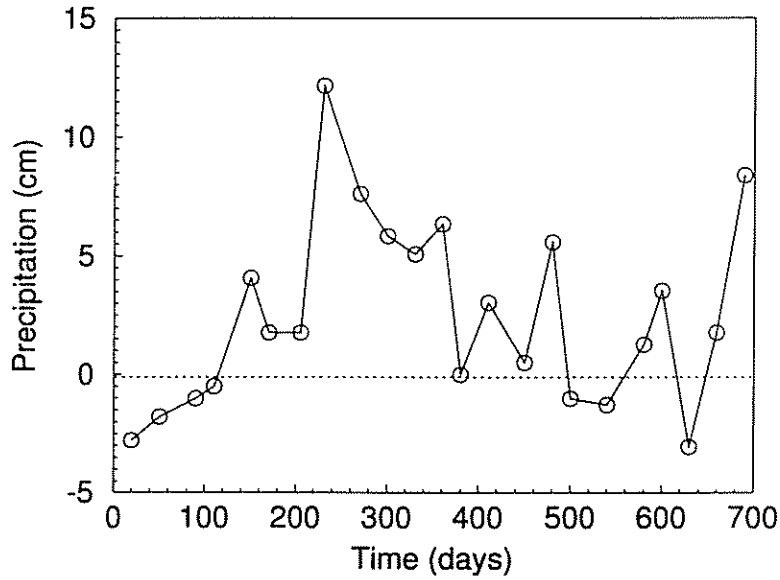

Figure 7. Precipitation departure data from the 50-year average

Mining-induced strains. The mining-induced strain magnitudes were evaluated from the procedure described previously, using the finite element model, and were incorporated directly into the analysis. The magnitudes, in this particular case, were constrained by the measured subsidence profile. The normalized distributions of mining-induced vertical and horizontal extensional strains are illustrated in Figures 8 and 9, respectively. The strain field is constrained in this *a posteriori* case by the form of the subsidence profile measured post-mining, although this is not a prerequisite for application of the method, since some estimate of R_m (ratio of elastic modulus for compressive elements to that for extensional elements) may typically be applied. This strain field

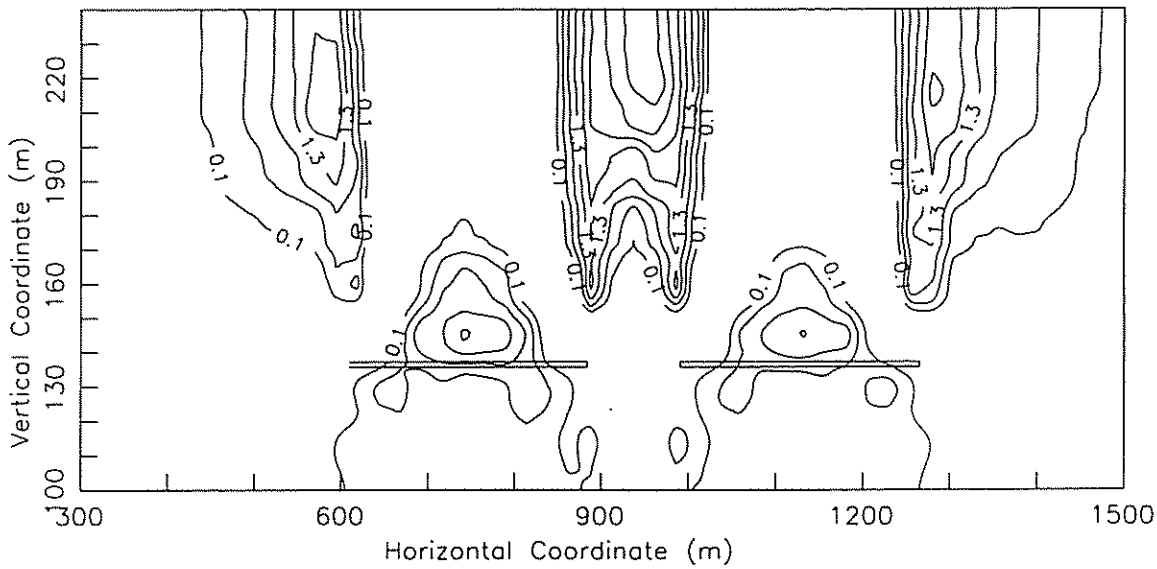

Figure 8. Contours of normalized horizontal strains ($1000\varepsilon_x$). Strains are normalized by multiplying by a factor of 1000. The two rectangular boxes represent the two panels

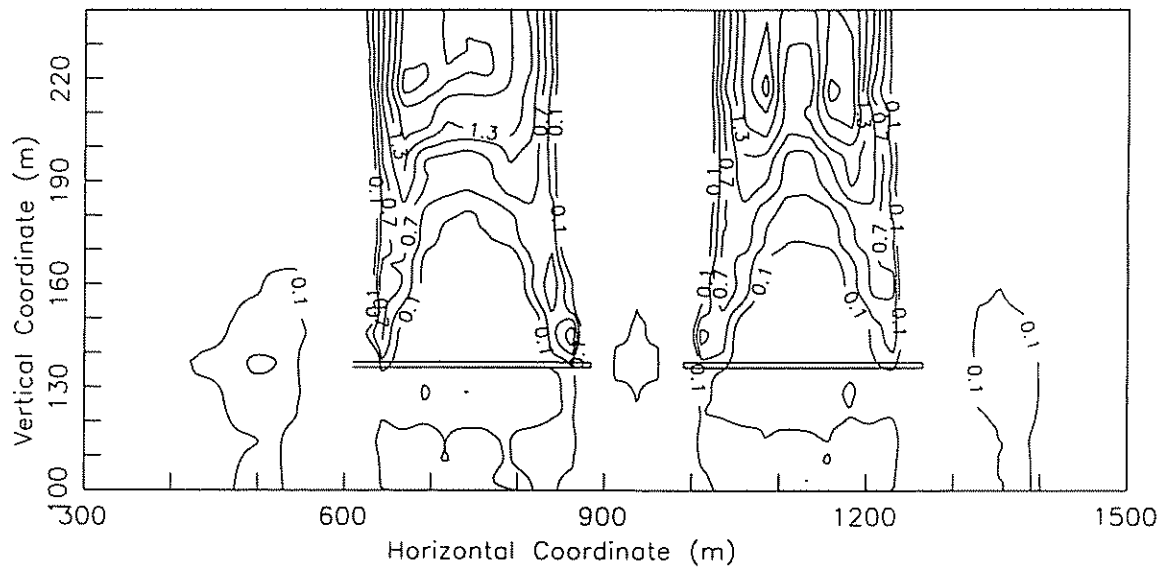

Figure 9. Contours of normalized vertical strains ($1000\varepsilon_y$). Strains are normalized by multiplying by a factor of 1000. The two rectangular boxes represent the two panels

is used to determine the revised post-mining hydraulic conductivity field and applied to define anticipated changes in water levels.

Pre-mining hydraulic conductivity. The pre-mining hydraulic conductivity magnitudes, considered representative of the sandstone overburden, were determined by using the maximum hydraulic conductivity values obtained at the site. All wells are open over their entire length and fully penetrate the uppermost shale, with portions completed in the underlying sandstone. Correspondingly, use of the maximum value as an

order-of-magnitude evaluation is appropriate. Pumping tests were run successively in wells 1 to 6 with interpretation assuming full penetration in confined aquifers. These drawdown and recovery pumping tests were performed on all wells before and after undermining to determine hydraulic conductivity parameters of the local, shallow geological units.

As shown in Figure 4b, the overburden is divided into three different units based on the lithology, as identified in Figure 2. These represent a lower shale layer (material 1) underlying an intermediate sandstone layer (material 2), which in turn underlies the uppermost shale layer (material 3). The maximum value of the hydraulic conductivities obtained at the site for material 2, $0{\cdot}7 \times 10^{-4}$ m/s, was used as the basic input, since all wells sample this unit. This higher conductivity of the sandstone is presumed to dominate the response of the wells to pumping tests. A hydraulic conductivity of $0{\cdot}7 \times 10^{-7}$ m/s was used for material 3, estimated from model calibration in the pre-mined geometry with initial measured water levels. For the lowermost shale unit (material 1), a lithology similar to the upper unit, a hydraulic conductivity of $0{\cdot}7 \times 10^{-8}$ m/s was used that reflects the influence of depth on conductivity (Walker, 1986). No tests were completed within this unit, and estimates were made from the known shale lithology and constrained by calibration studies from known post-mining pumpage from the longwall panel.

The hydraulic conductivity magnitudes represent aggregate parameters over the full vertical section of the respective wells, where the major flow zone is restricted to the underlying sandstone, enabling sandstone conductivities to be adequately defined, as reported above. High-end values of measured conductivity were used to represent the anticipated dominance of the more conductive units in the field testing results. In addition to the well-bore tests, calibration studies were completed to match pre-mining water levels using the conductivity of the lowermost shale layer as a variable, and are reported in Figure 13. Clearly, a number of variables remain unconstrained, including approximated magnitudes of infiltration; however, the shallow nature of the monitoring array results in near-surface effects dominating the response with low-order influence of the underlying impermeable unit. Correspondingly, the modelling results are not sensitive to the choice of hydraulic conductivity for the lower shale layers as it acts as an impermeable lower boundary for the evolving near-surface flow regime.

Fracture spacings. The fracture spacings for each of the materials should be available in order to close the system. From outcrop observations, they were estimated as 0·1 m for both materials 1 and 3 and 0·2 m for material 2. These are to be assumed representative and reasonable in the absence of corroborating core data, and represent second-order importance when compared, for instance, with sensitivity to conductivity measurements.

Modulus reduction ratios. The modulus reduction ratio, R_m, is the last of the required input parameters and remains critical in defining the sensitivity of the induced conductivity field to the estimated strain field. In order to determine the values of R_m, some constraint must be applied to the system. The flow rate entering the mine following the excavation of both panels is the best candidate. The flow rate provided by the mining company was about 0·03 m^3/s. The values of R_m determined through matching this flow rate are 0·95 for material 1, 0·10 for material 2 and 0·80 for material 3. Choice of these parameters is clearly non-unique, but is predicated on the anticipated response of the lithological units to straining and fracturing. The value of R_m is chosen as 0·95 for the lower shale unit and 0·80 for the upper shale layer because only a small part of the extensional strain is applied to the fracture system and results in the smallest possible change in conductivity. The difference between the two values represents the effect of depth. The value of R_m is chosen as 0·10 for the sandstone unit because a large part of the extensional strain is applied to the fracture system and precipitates the largest possible change in conductivity.

The post-mining hydraulic conductivity field, evaluated from the calculated strain field and Equations (2) and (3), was used directly to calculate the post-mining groundwater budget. Changes in hydraulic conductivity are illustrated in Figures 10 and 11. The log of the ratios of post-mining horizontal conductivity to pre-mining horizontal conductivity [$\log(R_{cx})$] are shown in Figure 10, and only the zones of increased

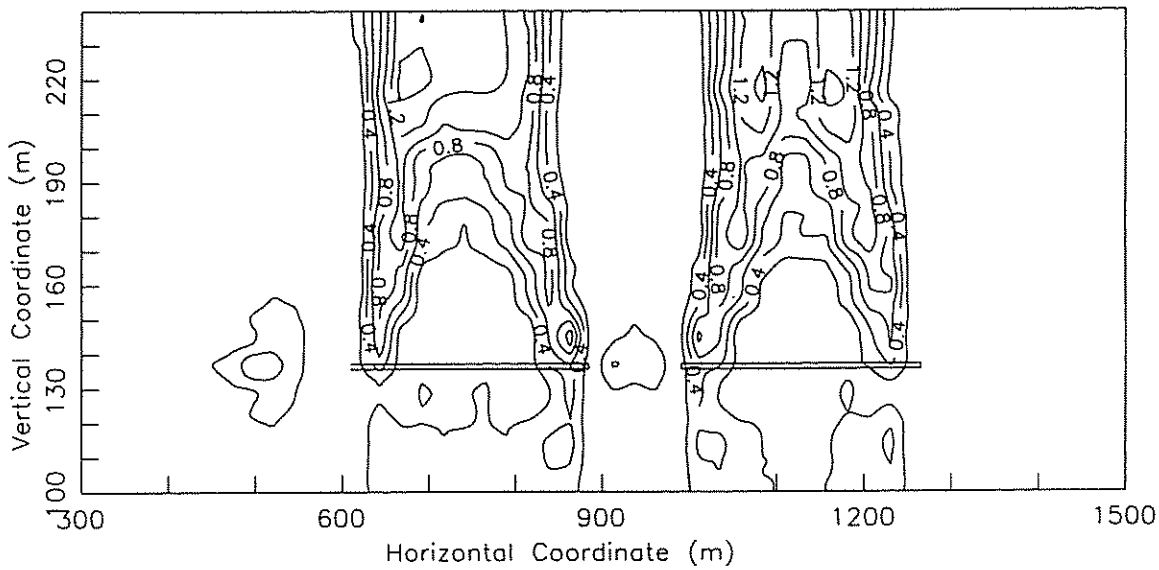

Figure 10. Contours of ratios of post-mining horizontal conductivity to pre-mining horizontal conductivity [$\log(R_{cx})$]. The two rectangular boxes represent the two panels

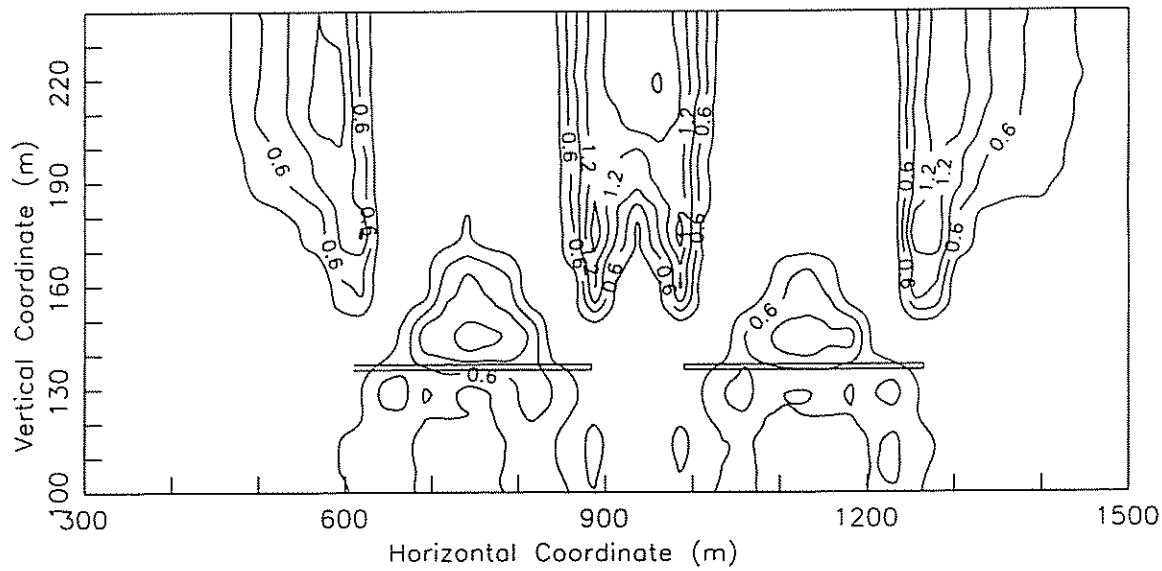

Figure 11. Contours of ratios of post-mining vertical conductivity to pre-mining vertical conductivity [$\log(R_{cy})$]. The two rectangular boxes represent the two panels

conductivity are plotted. The ratios of post- to pre-mining horizontal conductivities directly above the panels and at ground surface may increase by as much as a factor of 20. The log of the ratios of post-mining vertical conductivities to pre-mining vertical conductivities [$\log(R_{cy})$] are shown in Figure 11. Vertical conductivities above the gate roads, near the ground surface and at the two wings of the mining site may increase by as much as a factor of 40. The post-mining vertical conductivity in the caving zones may increase by a factor of 20 over the pre-mining vertical hydraulic conductivity. Although the overburden is considered to be initially homogeneous and isotropic, the strong heterogeneous and anisotropic conductivity field develops as a result

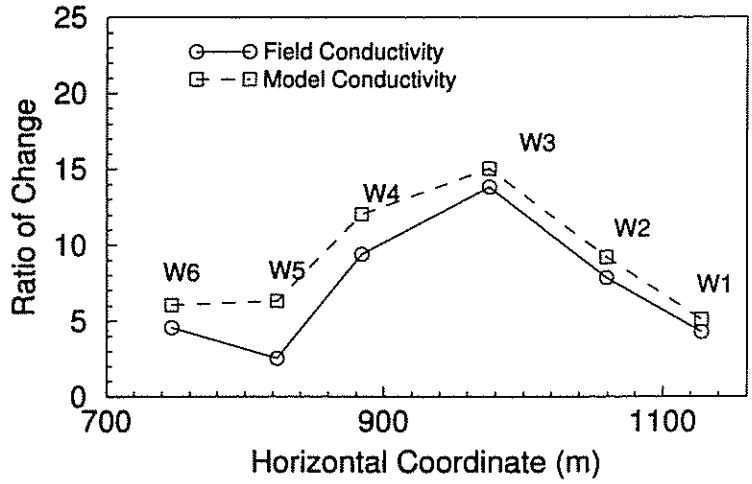

Figure 12. Comparison of model conductivity change ratios (R_{max}) with field ratios

of mining. The comparison between the evaluated ratios of the post-mining to pre-mining conductivities and the measured values is shown in Figure 12. The total change in the post-mining hydraulic conductivity, may be determined at the test locations (well locations) by summing the squares of the post- to pre-mining hydraulic conductivity ratios, R_{cx} and R_{cy}, as $R_{max} = \sqrt{\{R_{cx}^2 + R_{cy}^2\}}$. These results are compared with the field data in Figure 12. The ratios evaluated from the analyses compare favourably with the measured field ratios.

Groundwater tables were determined through evaluating the development of the phreatic surface following mining of both panels. Analyses were completed using a coarse mesh that covers the entire site response, and enables 'gross' evaluation of groundwater response, followed by a more detailed evaluation of the monitoring site area. For the large mesh, the calibration results for the pre-mining groundwater levels, and projected results for the post-mining behaviour, are illustrated in Figure 13. Under the applied boundary conditions, increased flow to the twin panels would result in a maximum water level drawdown of 3 m when the infiltration rate is set to zero. If infiltration is enabled at a rate of 0·25 m/y then the phreatic surface remains unaffected and the observed minimal impact on the groundwater system (at the regional scale) is adequately replicated. These calibration studies are not unduly influenced by the choice of conductivity

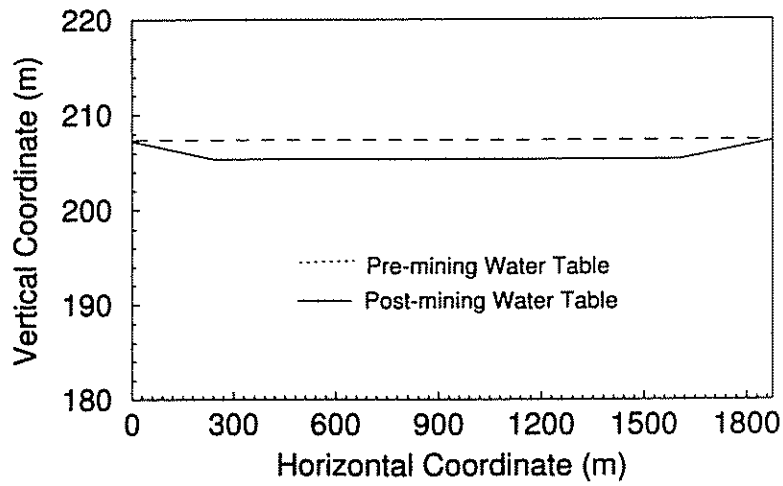

Figure 13. Model results of pre-mining and post-mining groundwater tables

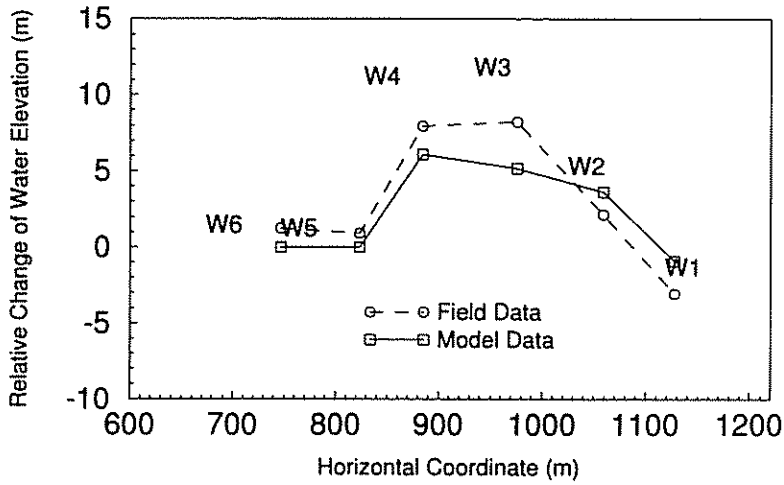

Figure 14. Relative change of water levels in monitoring wells. Datum set relative to original water level in well W6 at approximately 22·5 m below collar at ground surface

values for the lower shale layer, which is difficult to determine. The influence of the local topographic change on the post-mining groundwater table is simulated in the following small-scale groundwater model nested within the regional hydrological framework defined previously.

Local post-mining groundwater table fluctuations

Relative changes between the pre-mining and post-mining groundwater levels recorded in six monitoring wells are shown in Figure 14. Following completion of undermining of both panels, the equilibrium water levels in wells 5 and 6 recorded a slight rise, the levels in wells 2, 3 and 4 registered a more substantial rise of up to 8·2 m and the level in well 1 dropped approximately 3 m. This heterogeneous response may be explained purely by the anticipated changes in the distribution of hydraulic conductivity and the existing site topography. This requires that a small-scale view of the study area be taken, isolating the region monitored by the six wells. The form of this region is identified in Figure 15, describing the local topography and the appropriate applied boundary conditions.

Rise in the water table, post-mining, as illustrated in Figure 14, seems counter-intuitive given the large increases in hydraulic conductivity. However, wells where these changes are recorded are all located in the near-surface, underlain by relatively impermeable shales, and, most importantly (see Figure 4), are present

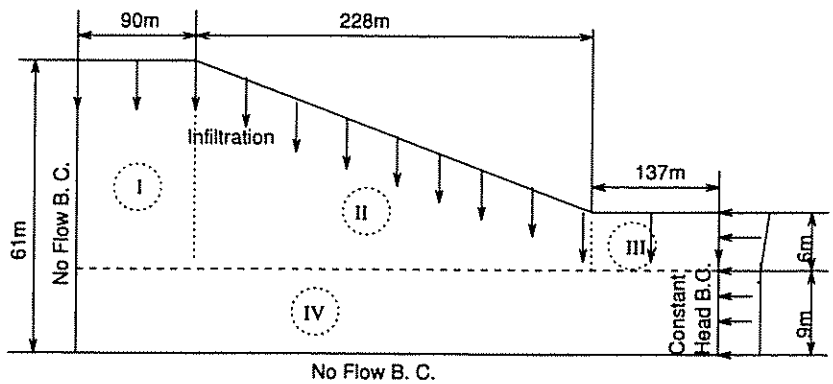

Figure 15. Small-scale FE model for flow simulation. Inset in Figure 4 defines location relative to the panels

on a shallow dipping hillside. Where water infiltrates into this section at a single prescribed rate, uniform increases in conductivity will cause steady-state upslope water levels to fall and downslope water levels to rise correspondingly. Thus a given flow rate is maintained at lower overall gradient in a body of increased conductivity. This adequately describes the mechanism, although the behaviour in this study is complicated by further levels of heterogeneity that develop locally within the hillslope.

The small-scale FE model is divided into four zones to represent the approximate distribution of post-mining hydraulic conductivities, as illustrated in Figures 10 and 11. This model represents the region between the centre-lines of both panels containing wells 5 and 6 within zone I, wells 2, 3 and 4 within zone II, and well 1 within zone III. No-flow boundary conditions are specified along the base and on the left side (the centre-line of panel No. 2) and constant head conditions are applied on the remaining vertical side (about 76·2 m away from the centre-line of panel No. 1). These no-flow conditions represent the impermeable underlying shale and a topographically induced local groundwater divide at the left side of the small model. The model is constructed of 326 nodes and 295 elements. Two different situations are simulated through this small-scale model. The same infiltration rate and pre-mining conductivities as the previous flow model define the anticipated pre-mining groundwater conditions, where the small-scale influences of topographically induced flows are accommodated. Secondly, the post-mining hydraulic conductivity magnitudes of Table II are incorporated to determine the anticipated post-mining groundwater levels. The post-mining hydraulic conductivity magnitudes are determined using Equations (2) and (3) and the constrained strain fields shown in Figures 8 and 9. Average magnitudes of horizontal and vertical conductivities are then utilized in the small-scale FE model as shown in Figure 15, representing the instrumented study site. Magnitudes of the hydraulic conductivity change most in extension, but are restricted in compression owing to constraints on the overclosure, or reclosure, of fractures. The post-mining hydraulic conductivities for zone IV, representing the major water-bearing layer, are assumed to be unchanged post-mining.

Table II. Post-mining conductivities and ratios of post- to pre-mining conductivities for the macro-scale model to define well response

Material	Post-mining conductivities		Post-mining ratios	
	K_x (m/s)	K_y (m/s)	R_{cx}	R_{cy}
1	$0{\cdot}7 \times 10^{-7}$	$0{\cdot}70 \times 10^{-8}$	1:1	1:10
2	$0{\cdot}7 \times 10^{-8}$	$0{\cdot}14 \times 10^{-7}$	1:10	1:5
3	$0{\cdot}7 \times 10^{-7}$	$0{\cdot}70 \times 10^{-8}$	1:1	1:10
4	$0{\cdot}7 \times 10^{-5}$	$0{\cdot}70 \times 10^{-5}$	1:1	1:1

The results are shown in Figure 16. The pre-mining water table is homogeneous and flat. However, the post-mining groundwater levels in the strongly heterogeneous and anisotropic conductivity field exhibit large, and apparently random, spatial variability, as is apparent in the local behaviour recorded in Figure 6. Some post-mining water levels are higher than those pre-mining, and others are lower, with no obvious pattern. It is apparent that the heterogeneous response results from the highly heterogeneous and anisotropic conductivity field developed following longwall mining. Relative changes in the simulated pre-mining groundwater levels and the simulated post-mining groundwater levels were compared with the measured data in Figure 14. Despite the significant levels of data uncertainty that existed at this site, a surprising agreement is evident between the measured and simulated response.

CONCLUSIONS

A methodology is presented for the determination of the regional and local effects of mining subsidence on the groundwater system. The methodology requires that subsidence-induced strains may be determined from

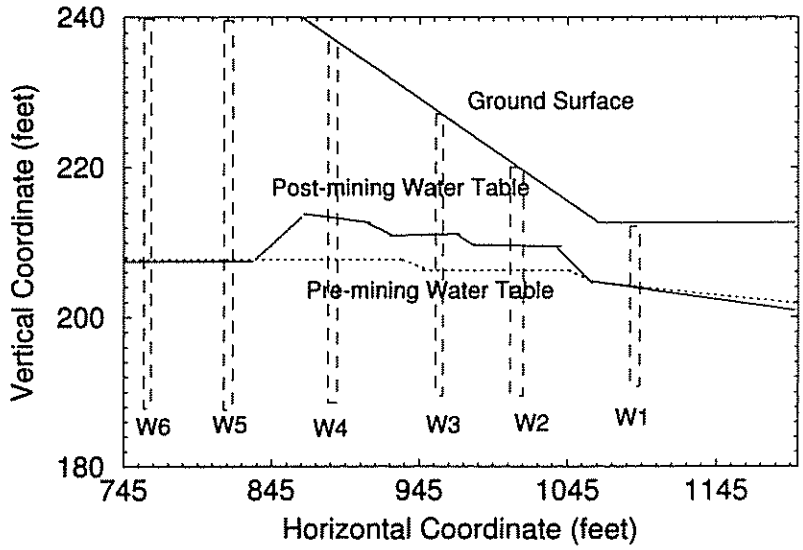

Figure 16. The small-scale model results of pre- and post-mining groundwater tables

forward modelling of the deformation processes using a non-linear finite element model. Data requirements for the model are minimal, requiring that maximum subsidence magnitudes are defined as the single 'curve-fitting' parameter. The displacement-controlled nature of subsidence, controlled primarily by the thickness of the extracted seam and overburden geometry, makes the strain field insensitive to material parameters such as elastic and inelastic moduli or shear strengths. With the evaluation of the strain field, changes in conductivity may be evaluated straightforwardly from knowledge of the strain field, initial conductivities and fracture spacing parameters. This model is relatively robust, requiring only parameters that are readily measured in the field, or may be estimated within reasonable bounds. From knowledge of the revised conductivity field, changes in groundwater budget and local changes in the groundwater flux field may be determined.

From this comparative study, measured changes in the hydraulic conductivity field match well with those evaluated independently through the application of this robust methodology, as was apparent in previous studies (Elsworth and Liu, 1995). From the results it is apparent that a strong heterogeneity of the conductivity field develops from subsidence-induced displacements, as shown in Figures 10 and 11. These anthropogenic effects are induced upon the already slightly heterogeneous conductivity field that results from tectonism, diagenesis and geological exhumation. In this respect it is surprising that the normal homogenization methods applied in evaluating the results of *in situ* conductivity tests at field scale are successful, since the large variability that develops in this study exerts strong control on the resulting phreatic surface profile. It is also not surprising that homogenization may perform poorly in representing transport behaviour.

The case study evaluated in this work is reasonably constrained by field and operational data documenting conductivity test results and bulk flow magnitudes through the system, post-mining. This constraint is applied to define the boundary conditions applicable to the small-scale flow regime present on one hillslope above the panels. The changes in hydraulic conductivity manifest in the hillslope environment are more strongly related to location relative to the panel, than to the original 'pre-mining' spatial conductivity distribution. The development of zones of differing conductivity in response to the strain field is corroborated by comparing the measured and calculated results, which appear consistent in form (Figure 12) if not directly in magnitude. Secondary corroboration of the successful match between field-measured and model-evaluated magnitudes is the ability to match changes in water budgets and changes in the post-mining

groundwater surface. The observed post-mining water level fluctuations are closely replicated by applying the small-scale groundwater FE model to the pre-mining conditions. The hydraulic behaviour of this hillslope segment reveals an extremely complex response, all aspects of which are explicable in terms of the projected changes in hydraulic conductivity distributions. This capability is extremely important in enabling the influence of mining on water supplies to be adequately evaluated.

ACKNOWLEDGEMENTS

This work has been supported by the National Science Foundation under Grant No. CMS-9209059, and by the National Mined Land Reclamation Center under Grant No. CO388962. This support is gratefully acknowledged. The rigorous and constructive comments of two anonymous reviewers are similarly acknowledged.

REFERENCES

Bathe, K. and Khoshgoftaar, M. R. 1979. 'Finite element free surface seepage analysis without mesh iteration', *Int. J. Num. Meth. Anal. Meth. Geomech.*, **3**, 13–22.

Booth, C. J. 1992. 'Hydrogeologic impacts of underground (longwall) mining in the Illinois basin', Peng, Syd S. (Ed.), *Proc., Third Workshop on Surface Subsidence due to Underground Mining*, West Virginia University, pp. 507–515.

Elsworth, D. and Liu, J. 1995. 'Topographic influence of longwall mining on groundwater', *Groundwater*, **33**, 786–793.

Elsworth, D., Liu, J., and Ouyang, Z. 1994. 'Some approaches to determine the potential influence of longwall mining on groundwater resources', *3rd International Conference on the Abatement of Acidic Drainage, Pittsburgh, PA.*

Liu, J. 1994. 'Topographic influence of longwall mining on groundwater supplies', *MS Thesis*, Department of Mineral Engineering, Pennsylvania State University, 113 pp.

Matetic, R. J. 1993. 'An assessment of longwall mining-induced changes in the local ground water system', *FOCUS Conference on Eastern Regional Ground Water Issues, 27–29 September 1993.*

Matetic, R. J. and Trevits, M. A. 1990. 'Case study of longwall mining effects on water wells', Preprint 90-141. *Society of Mining, Metallurgy and Exploration, Inc. Annual Meeting, Salt Lake City, UT. Trans.*, **292**, 1814–1818.

Matetic, R. J. and Trevits, M. A. 1992. 'Longwall mining and its effects on ground water quality and quantity at a mine site in the Northern Appalachian coalfield', *Proceedings, FOCUS Conference on Eastern Regional Ground Water Issues, Boston, MA*, pp. 573–587.

Matetic, R. J., Liu, J., and Elsworth, D. 1995. 'Modeling the effects of longwall mining on the ground water system', *Report of Investigations 9561. US Bureau of Mines, United States Department of the Interior*, 14 pp.

Neate, C. J. and Whittaker, B. N. 1979. 'Influence of proximity of longwall mining on strata permeability and ground water', *Proc., 20th US Symposium on Rock Mechanics, The University of Texas at Austin, 4–6 June, Texas, Austin*, pp. 217–224.

Ouyang, Z. and Elsworth, D. 1993. 'Evaluation of groundwater flow into mined panels', *Int. J. R. Mech. Min. Sci. Geomech. Abstr.*, **30**(2), 71–79.

Walker, J. S. 1986. 'Case study of the effects of longwall mining induced subsidence on shallow ground water sources in the Northern Appalachian coalfield', *Report of Investigations 9198, US Bureau of Mines, United States Department of the Interior*, 22 pp.

